DOI: http://dx.doi.org/10.12989/was.2010.13.2.127
Wind and Structures, Vol. 13, No. 2 (2010) 127-144

Special Issue paper on Windborne Debris

Aerodynamic forces on fixed and rotating plates

P. Martinez-Vazquez[1]*, C.J. Baker[1], M. Sterling[1], A. Quinn[1] and P.J. Richards[2]

[1]*School of Civil Engineering, University of Birmingham, UK*
[2]*Department of Mechanical Engineering University of Auckland, New Zealand*

(Received September 8, 2009, Accepted November 3, 2009)

Abstract. Pressure measurements on static and autorotating flat plates have been recently reported by Lin *et al*. (2006), Holmes, *et al*. (2006), and Richards, *et al*. (2008), amongst others. In general, the variation of the normal force with respect to the angle of attack appears to stall in the mid attack angle range with a large scale separation in the wake. To date however, no surface pressures have been measured on auto-rotating plates that are typical of a certain class of debris. This paper presents the results of an experiment to measure the aerodynamic forces on a flat plate held stationary at different angles to the flow and allowing the plate to auto-rotate. The forces were determined through the measurement of differential pressures on either side of the plate with internally mounted pressure transducers and data logging systems. Results are presented for surface pressure distributions and overall integrated forces and moments on the plates in coefficient form. Computed static force coefficients show the stall effect at the mid range angle of attack and some variation for different Reynolds numbers. Normal forces determined from autorotational experiments are higher than the static values at most pitch angles over a cycle. The resulting moment coefficient does not compare well with current analytical formulations which suggest the existence of a flow mechanism that cannot be completely described through static tests.

Keywords: aerodynamic force coefficients; wind effects; debris.

1. Introduction

The determination of aerodynamic effects on wind-borne debris requires the knowledge of the flow-structure interaction. This can be achieved through physical measurements of the variation of pressures over the object’s area exposed to wind to allow full description of the external forces acting on it. Plate-like objects have been identified as representative of a variety of structural attachments of common use in engineering design. Therefore the definition of the aerodynamic forces on fixed and auto-rotating plates would provide an extended view on this phenomenon for a wide range of theoretical and practical applications. Experimental measurement of surface pressure on plates has been reported since the first half of the last century, e.g. Flachsbart (1932) and Riabouchinsky (1935). The growth of the aircraft industry encouraged further development, mainly orientated towards the study of missiles, slender wings, and aerofoils, see for example, Daniels (1970), Cohen (1976), and Neumark (1963). The case of flat plates that resemble common shapes driven by strong winds was given further experimental attention by Iversen (1979), Tachikawa

* Corresponding Author, Research Fellow, E-mail: p.vazquez@bham.ac.uk

(1983), and Lugt (1983). These contributions enabled the development of analytical models to predict the trajectory of flight of objects, classified after Wills, *et al.* (2002) as compact, sheet-type, and rod-type debris – see for example Holmes, *et al.* (2006), Baker (2007), and Richards, *et al.* (2008). These models assume that the forces on the plates are those measured in stationary experiments, magnified in some way to allow for autorotating effects, and generally make use of the approximation given in Tachikawa (1983) for the autorotation magnification. However, apart from Tachikawa's work, there is no evidence regarding the instantaneous variation of surface pressures during stable autorotation. This investigation focuses on the determination of static and autorotating pressure coefficients for plates held at various combinations of pitch and yaw angles for three wind velocities: $U=5$, 7.5, and 10 m/s. Force coefficients were computed through a series of wind tunnel tests carried out at The University of Auckland, New Zealand.

The paper has been organised in five sections. Section 2 describes the experimental arrangements, while Section 3 presents the results relating to the static and auto-rotational experiments. Section 4 discusses in detail the effect of the auto-rotation on the measured coefficients, with closing remarks and conclusions given in Section 5.

2 Experimental setting

2.1. Test-sheet

The test-sheet, representing a typical roof cladding panel, is a piece of polystyrene of 1m square, 2.5 cm thick and weighing 2.7 kg. A maximum tension stress of 80 kN/m^2 produced by bending was estimated for the extreme edge of the board's section, whilst 1.4 kN/m^2 was estimated for shear effects. The resistance of polystyrene ranges between 46 ~ 60 kN/m^2 for tension and it is approximately 50 kN/m^2 for shear (Gnip, *et al*. 2007). The base polystyrene material is thus able to withstand nearly 50% of tension and 100% of shear stresses. An adherent film with tension resistance of 600 kN/m^2 was thus placed over its surfaces in order to provide additional capacity.

The mass of the sheet-debris is important in determining the trajectory of flight when submitted to a given wind velocity profile. Using data from Tachikawa (1983) and Baker (2007) an autorotation frequency of 1 Hz and a time of flight of approximately 1s were predicted. This resulted in a Tachikawa Number ($Ta=\rho U^2 A/(2\,mg)$) of 2.31 for a wind speed of 10 m/s. This check was carried out in order to ensure that the test-sheet will tumble at least once during auto-rotational motion or during free flight experimentation (the results of which are not considered below) so that surface pressures will be available for angles between 0º ~ 360º. This data thus will enable the trajectory model outlined in Martinez-Vazquez, *et al*. (2009a) to be calibrated.

2.2. Pressure transducers

Twenty four pressure transducers were located on the test-sheet and arranged to cover the regions of expected peak pressures and suctions, i.e., along bisecting perpendiculars, edges and corners. Fig. 1 shows the distribution of sensors and data loggers and also the typical position of a sensor within the thickness of the board. The sensors with the polystyrene protection were fitted into square sections previously cut out from the board, placing the wiring over the surfaces oriented towards the corresponding data logger, which were positioned along the borders of the specimen in such a way

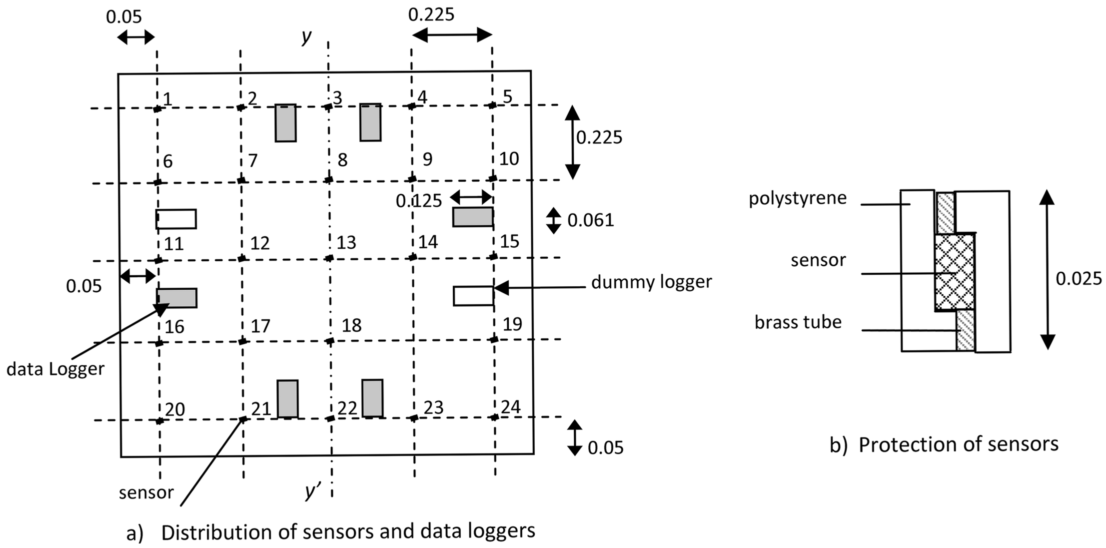

Fig. 1 (a) Distribution of sensors and data loggers and (b) sensor fitted within the thickness of the test-sheet

that their mass was uniformly distributed.

Compatible pressure sensors and portable data loggers were selected for the experiment. Differential pressure transducers manufactured by Sensortechnics with output voltage within 0.25 ~ 4.5 V, pressure range 0 ~ 2.5 mbar, and resolution of 12 bit, were used. The test-sheet was submitted to wind velocities up to 10 m/s, from these values a peak pressure of the order of 60 N/m^2 was estimated, corresponding to a surface pressure coefficient of 1.0. This value was suitable for the range of pressure accepted by the sensor and also for the resolution which represented 4×10^{-4} times the predicted peak pressure. For the data logger a portable card manufactured by Omni instruments (XR440-M) was considered suitable to work in combination with the sensors. One data logger supports 4 sensors, accepts an input signal of 0 ~ 5 V dc, and it provides a resolution of 8 ~ 12 bits with a maximum sampling frequency of 200 Hz. The device has a storage capacity of 129024 readings distributed in 4 channels working at 8 bits resolution; it has its own battery from which it can power to the pressure sensors. Its dimensions are $120 \times 61 \times 24$ mm, and it weighs 156 g. After testing the data from the logger can be downloaded to a PC via an interface cable.

2.3 Wind tunnel facilities

The experiments were carried out at the University of Auckland, New Zealand. In this facility the air is blown through a 3.5 m square nozzle towards an open area for testing with a turntable on the floor. Wind speeds $U = 5$, 10 m/s were selected for the static and $U = 5$, 7.5, 10 m/s for auto-rotational tests. The test duration was approximately 36 minutes for each static experiment, with a sampling frequency of 10 Hz which allowed several cases to be fitted into any one test period. The corresponding experimental period and sampling frequency for the auto-rotating tests was ~120 s and 200 Hz respectively. The sampling frequencies were chosen in order to provide data at every 0.1 s in static runs and at about every 2° for auto-rotation runs.

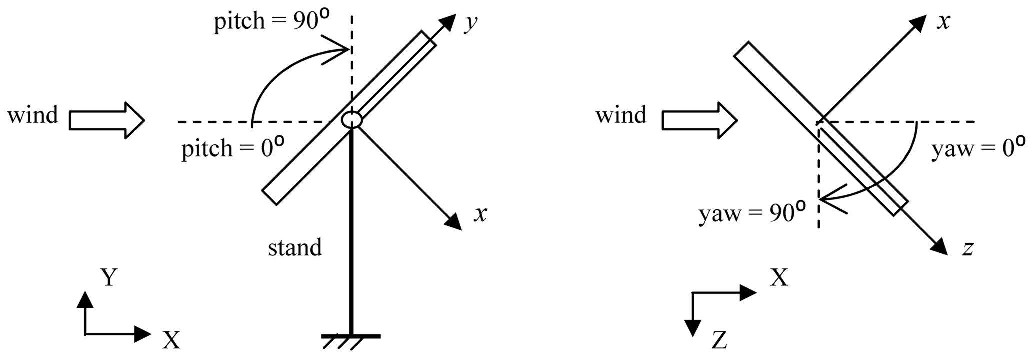

a) lateral view b) plan view

Fig. 2 Definition of (a) pitch angle, (b) yaw angle, local and global coordinates

2.4 Supporting system

Two metallic frames of height 1.5 m were built to support the test-sheet. The test-sheet was fitted into an aluminium frame which in turn was connected to the lateral stands via metallic pins. A mechanism for static and auto-rotating tests was implemented which consisted of two parallel plates connected through bearings and bolted in place every 15°. This arrangement allowed the plate to adopt the static positions by varying the pitch angle whilst yaw angle variation was given by rotating the base platform. The definition of local and global coordinates, pitch and yaw angle is given in Fig. 2. The plate was allowed to auto-rotate by releasing the parallel plates at the bearings. This supporting system caused some disturbance on static pressure measurements taken on the lower half of the board, mainly due to the blockage produce by the vertical stands. Inaccuracies caused by this effect were corrected during analysis as described in Section 3.

2.5 Cases for testing

The wind tunnel tests were divided into two categories: static (test-sheet restricted from translation and rotation) and auto-rotational (only rotation around the local axis z was permitted – see Fig. 2). Rotation of the board around the global Y and Z axis defines yaw and pitch angle, respectively - zero pitch and yaw corresponds to the flow normal to the larger face of the plate as indicated in Fig. 2. The pitch and yaw angles were varied from 0~90° in 15° increments with an additional run at the pitch angle where the stall region was detected. For auto-rotation tests the board was released at an angle of 15° clockwise from a horizontal plane. Additional details relating to this experiment can be found in Martinez-Vazquez, *et al*. (2009b).

3. Static tests

The first group of tests consisted of combinations of pitch and yaw angles within the range 0°~ 90° at every 15°. Preliminary results from the investigation showed the stall behaviour at the mid pitch angle range, and therefore additional data were collected at the intermediate angle of 37.5°. Raw

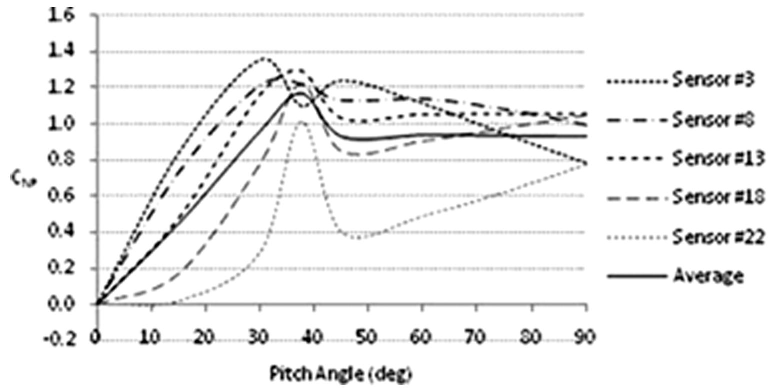

Fig. 3 Net pressures for a group of sensors all pitch angles at 90° yaw, $U = 10$ m/s

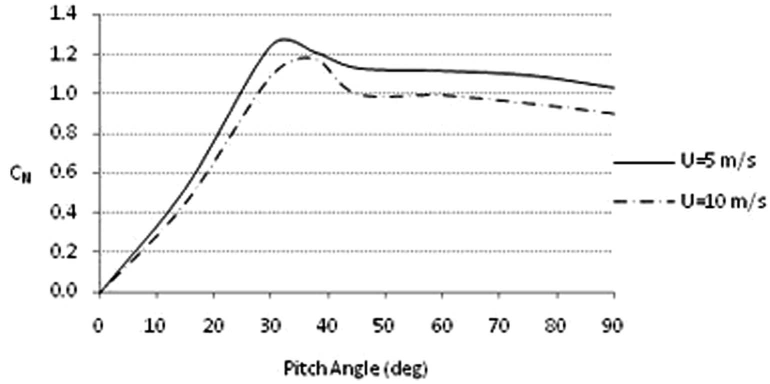

Fig. 4 Normal force coefficients all pitch angles at 90° yaw, $U = 5$, 10 m/s

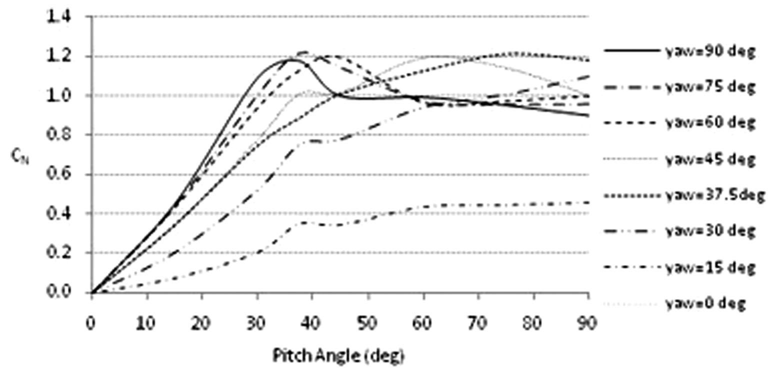

Fig. 5 Normal force coefficients all pitch and yaw angles, $U = 10$ m/s

data collected during testing were numerically processed in order to correct imprecision caused by blockage effects in the tunnel. Such correction consisted of establishing symmetry conditions on data series from sensors located at the bottom half of the board such that their mean value tended towards the average registered at the corresponding sensor in the upper half. The correcting factor for symmetry was linearly varied from its maximum value when the stands were aligned with the test-sheet held parallel to the flow (pitch and yaw angles equal to 90°, 0°, respectively) to a value equal to 0 when the board was held horizontal and the chord length was parallel to the flow (pitch and yaw angles equal to 0°, 90°, respectively). The resulting static force coefficients are shown in Figs. 3~5. Fig. 3 shows how the net pressure coefficients, $C_{NP}=P/(\rho U^2/2)$ (where P is the local pressure), vary with pitch angle for sensors located along the vertical axis of the board for wind velocity U=10 m/s. These sensors are labelled in Fig. 1 as #3, #8, #13, #18, and #22 – Fig. 3 also shows the average value for these sensors.

From Fig. 3 it is noticeable that all curves stall at a range of angles between 25°~45°. The asymmetry in the pressure distribution for intermediate pitch angles (for example at 25° pitch) has been captured by the pressure at opposite symmetric positions, e.g. sensor#3 / sensor #22, sensor #8 / sensor #18. The pressure values at these positions tend to similar values at pitch angle equal to 90° where minimum asymmetries are observed. The average normal pressure computed from this sample is similar to the normal force coefficient presented below, where the contribution of all sensors over the area is included.

Measured normal coefficients, $C_N = F_N/(\rho U^2 A/2)$ – where F is the total force and A the area of the board, for 90° yaw angle and U=5, 10 m/s, are presented in Fig. 4. The flow around the board stalls within the interval pitch angle 25°~45° with slightly higher values for U=5 m/s than for U= 10 m/s. Holmes, *et al.* (2006) and Richards, *et al.* (2008) reported peak values of about 1.6 at the stall region and a constant value of about 1.2 for angles of attack above 45°, i.e. a rather better defined stall characteristic than shown in Fig. 4. The Reynolds numbers, defined as $R_e = \rho UL/\mu$- where μ represents dynamic viscosity and L is a characteristic dimension of the board (e.g. the width), are 3.34×10^5 and 6.69×10^5 for U=5 m/s and 10 m/s, respectively.

The differences observed in Fig. 4 might be the result of higher turbulence in the approaching flow when increasing the wind velocity. For example, the net pressures registered at sensor #13 at the combination pitch, yaw angle={90°, 90°} are C_{NP}=1.22, 1.07, for U=5, 10 m/s, i.e. a lower surface pressure has been registered at the same point by increasing the wind speed. Fig. 5 shows the normal force coefficients C_N for all yaw angles plotted against pitch angle for U=10 m/s. It can be seen in this figure that all curves stall within the interval 25°~60°, i.e. this effect was observed at slightly different angles for yaw positions below 90°. It can also been observed that the value of the force coefficient for any combination pitch, yaw angle (p^o, q^o) is the same if the pitch and yaw angles are interchanged, i.e. $C_N(p^o, q^o)=C_N(q^o, p^o)$ indicating that the correction of blockage effects in the raw data tend to reflect ideal flow conditions where pressure measurements that result from varying the pitch angle only should be expected to be the same than those obtained by varying the yaw angle to give the same angle of attack.

The position of the centre of pressures was determined from static measurements for the range of angles of attack $0^o <= \varepsilon <= 90^o$ at constant yaw angle =0°. The ordinate of this point, y_{cp} is presented in Fig. 5 as a fraction of the chord length L of the test-sheet. The value of y_{cp} is similar for U=5, 10 m/s for pitch angle over 15°, with an increasing difference as ε approaches to zero, where the estimated values are y_{cp}/L=0.35, 0.25 for U=5, 10 m/s respectively. Based on this data the exponential expression given in Eq. (1) is assumed – where ε is given in radians. Eq. (1) was formulated empirically based on the form of the curves obtained with experimental data, using a fixed point of 0.3 for zero angle of attack to represent the midpoint between the curves for U=5, 10 m/s. Fig. 6 also shows how the experimental and exponential curves compare to equivalent approaches suggested in Holmes, *et al.* (2006), and Richards, *et al.* (2008).

$$\frac{y_{CP}}{L} = \frac{3}{10}\varepsilon^{-3\varepsilon/2} - \frac{\varepsilon}{18\pi} \tag{1}$$

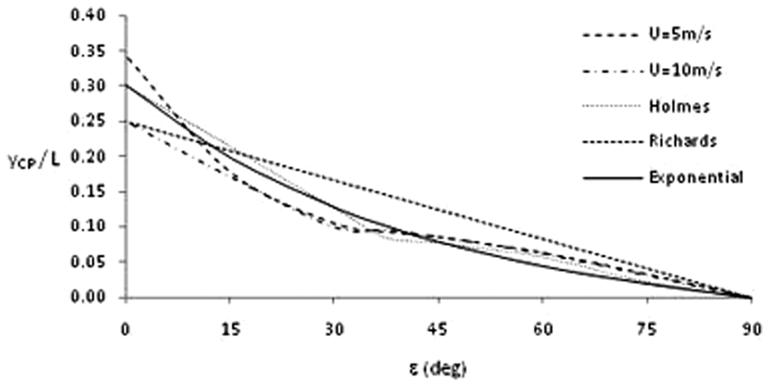

Fig. 6 Position of the centre of pressure determined through various experimental approaches

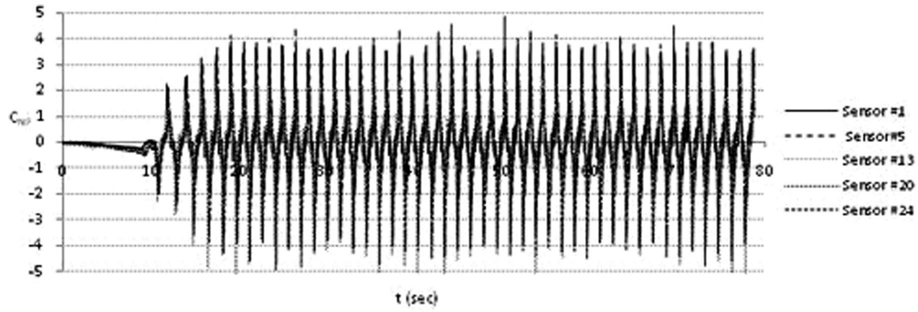

Fig. 7 Time series of net force coefficients at four sensors on the board, $U = 7.5$ m/s

4. Auto-rotation

Two stages can be identified before a plate settles into a stable rotation. These are when the plate acquires enough angular momentum during the supporting period (defined in Lugt (1983) as torque acting in the direction of autorotation) in order to overcome the retarding period, followed by the transition where the peak pressure increases to a nearly constant value. In this experiment, the plate was released at a pitch angle of about 15° from its horizontal position passing the initial stages relatively soon, as shown in Fig. 7. Every autorotational test lasted about 107 seconds, i.e., 30 s for the initial over run of the wind flow plus 77 s which covered the autorotational event. Only the last 30 seconds were considered for analysis in order to guarantee that the flow was fully developed and the board was under stable autorotation. Fig. 7 shows the normal pressure coefficient from the moment in which the board was released until it freely rotated, i.e., the last 77 s. It shows the four sensors at the corners: #1, #5, #20, and #24, plus sensor #13 which is located at the centre of the board, see Fig. 1. Fig. 8 shows a five-second segment of the series shown in Fig. 7 in order to observe the various pressure registered by these sensors.

Computation of instantaneous forces and moments on the plate was achieved through an integration of the net pressure coefficients. The autorotational data series had to be corrected due to a time delay of a fraction of a second detected in some of the logging cards used for the experiment. This alignment consisted in defining the peak value of a ten point moving averages (in

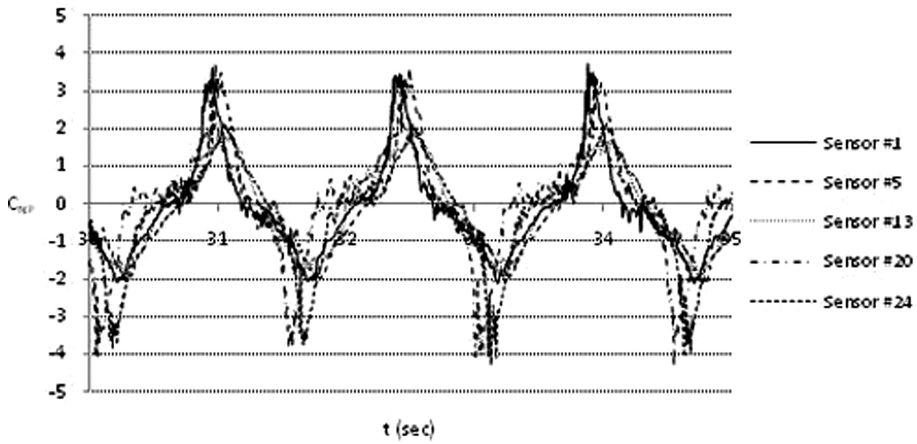

Fig. 8 Five-second series of net force coefficients at four sensors on the board, $U = 7.5$ m/s

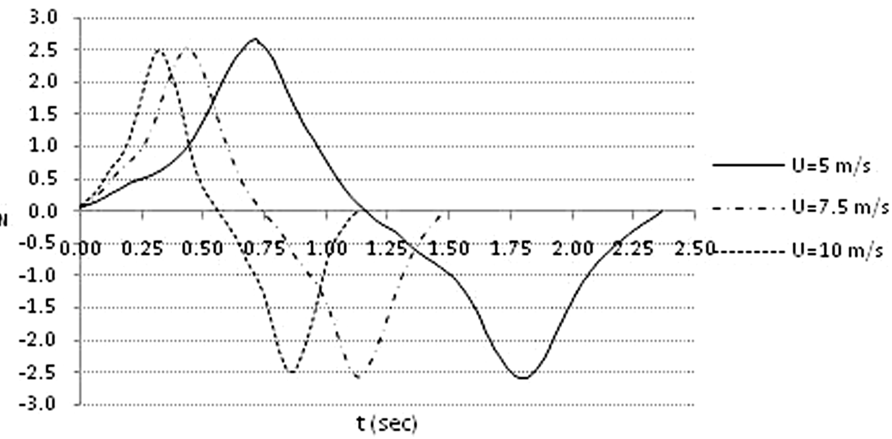

Fig. 9 Normal force coefficient on averaged cycles, $U = 5$, 7.5, 10 m/s

order to avoid local spurious peaks) in the first cycle after the plate was released - $t \approx 12$ seconds. At this point the angular speed was rather low, so a peak positive was expected to occur at the same time for all sensors. Using the aligned series, force coefficients were observed on an averaged characteristic cycle. These cycles for the normal force coefficient acting on the board are shown in Fig. 9 for the three testing velocities, $U=5$, 7.5, and 10 m/s.

It is observed in Fig. 9 that the averaging process has reduced the peaks from all sensors, i.e. the force coefficients $C_N \approx 4$ presented in Figs. 7, 8 are local maxima. From the above data shown in Fig. 9 the average rotation periods can be inferred: 2.36 s, 1.48 s, and 1.12 s, for wind velocities of $U=5$, 7.5, and 10 m/s, respectively. Tachikawa (1983) uses the tip velocity in order to define the frequency of rotation of square plates and application of his method leads to the calculation of theoretical periods of rotation of 1.96 s, 1.31 s, and 0.98 s. The difference in these values can be attributed to frictional effects at the bearings. This is considered further in a dynamic analysis of the experimental situation described in Appendix A.

It is possible to compare the overall normal force coefficients determined through static and auto-

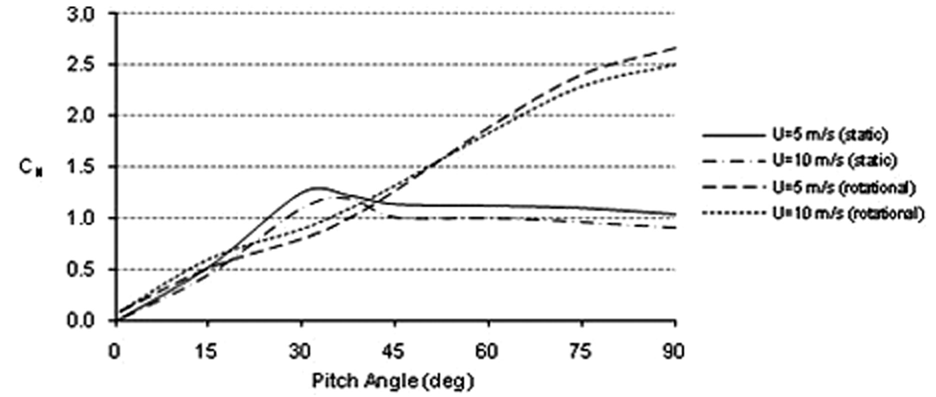

Fig. 10 Static and autorotational force coefficients

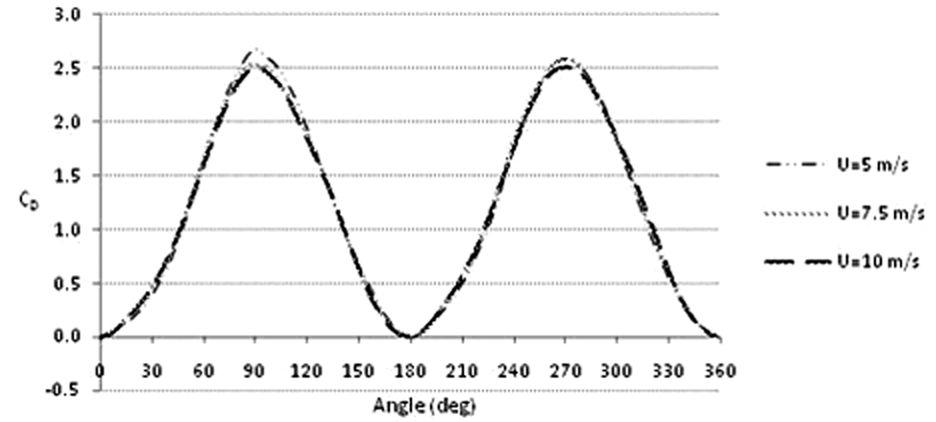

Fig. 11 Drag coefficient, $U=5$, 7.5, 10 m/s

rotational experiments. Fig. 10 shows values of C_N for $U=5$, 10 m/s for these two types of test in the range of pitch angle $0^o \sim 90^o$. The present data indicates that static forces are higher within the stall region, otherwise auto-rotational forces dominate. This figure also shows that static coefficients for $U=10$ m/s are consistently lower than those for $U=5$ m/s, which does not happen in autorotation where the curves switch their relative position at 50^o pitch angle. The differences depicted in Fig. 10 suggest that static and auto-rotational forces might be the result of different flow mechanisms.

The derived auto-rotational drag, lift and moment coefficients are presented in Figs. 11~13, and are formally defined as: $C_D = F_{NX}/(\rho U^2 A/2)$, $C_L = F_{NY}/(\rho U^2 A/2)$, $C_M = T/(\rho U^2 L^3/2)$ - where T is the acting torque, L is a characteristic length (e.g. chord length), and F_{NX}, F_{NY} are the total forces resulting from integrating surface pressures acting in the X and Y global directions, respectively, as indicated in Fig. 2 - note that whilst Figs. 9 and 10 show the normal coefficient in local coordinates, drag and lift are presented in global coordinates. Figs. 11~13 show the effect of $R_e = \{3.34\times10^5, 4.46\times10^5, 6.69\times10^5\}$ when varying $U = \{5, 7.5, 10 \text{ m/s}\}$, this effect is more clear in the moment coefficients shown in Fig. 13 (although it must be noted that moment coefficients are based on the instantaneous variation of pressures over the surface of the board rather than on averaged forces, as drag and lift coefficients). In Fig. 13, where positive torque is defined as to increase the pitch angle,

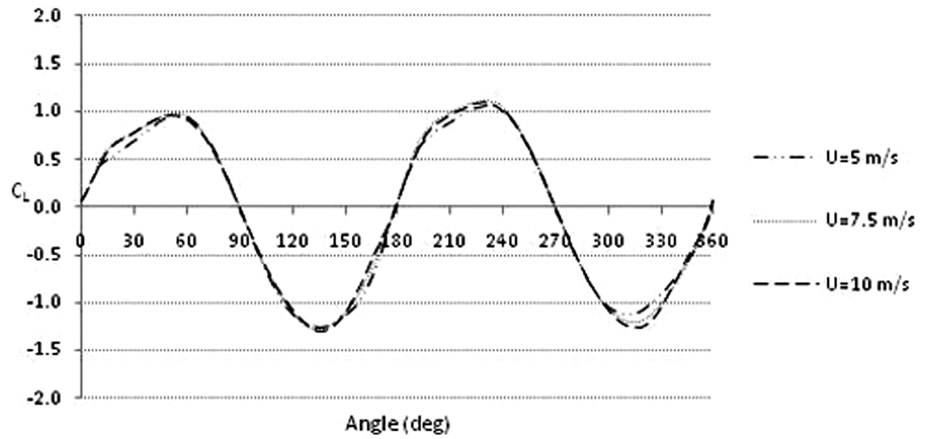

Fig. 12 Lift coefficient, $U = 5$, 7.5, 10 m/s

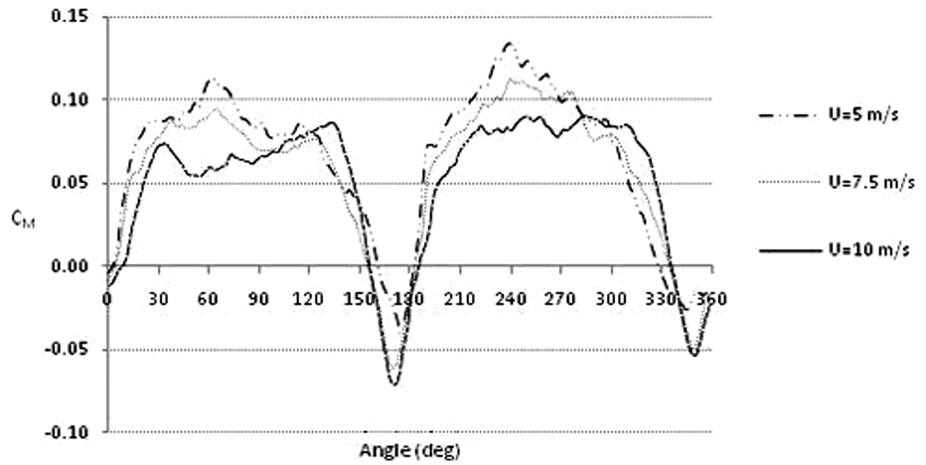

Fig. 13 Moment coefficient, $U = 5$, 7.5, 10 m/s

it is clear why the plate undertakes stable auto-rotation. However, since the rotational speed is not constant throughout a cycle, an approximate function to define the moment coefficient was calculated from the solution of the equation of motion that approximates the rotational movement of the test-sheet, see Appendix A. Once the variation of angular velocity was determined, data collected in the time domain could be analysed and then represented in angular units as in Figs. 11~13.

It is interesting now to observe how the measured moment coefficients compare with the quasi-steady values, i.e. forces derived from the normal force coefficients presented in Fig. 9 combined with the exponential variation of the position of the centre of pressure formulated in Eq. (1) and represented in Fig. 6. Fig. 14 show this comparison for U=7.5 m/s only, although all three levels of wind velocity show similar characteristics. The difference between these two sets of data is here referred to as co-rotation. The rotational scenario depicted in this figure suggests the existence of two mechanisms, quasi-steady and co-rotation, which are almost symmetric with regard to zero values. These mechanisms would define the total torque acting on the rotating plate. From the present analysis it appears that co-rotation is consistent for the three Reynolds numbers studied. This is shown in Fig. 14 in which curves are

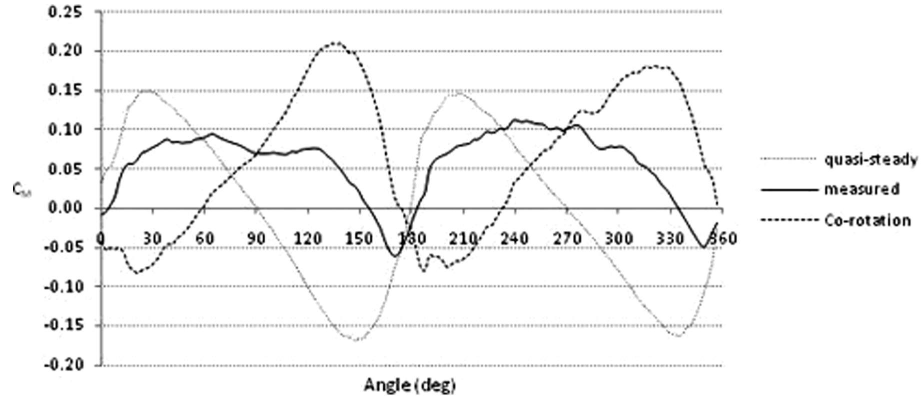

Fig. 14 Autorotational scenario, $U = 7.5$ m/s

Table 1 Index of variation of areas for subsequent cycles of acting normal pressure

	$I_v = \sigma/\mu_f$, U=5 m/s	$I_v = \sigma/\mu_f$, U=7.5 m/s	$I_v = \sigma/\mu_f$, U=10 m/s
Pressure range (+)	0.0133	0.0156	0.0142
Pressure range (–)	0.0110	0.0162	0.0168

characterised by a switch between positive and negative values with well defined intervals.

Lugt (1983) noted that under certain conditions a rotating plate may trap a vortex which would then be released at a constant rate or after several revolutions, depending on the frequency of rotation of the plate. One possible way to estimate the rate at which vortices are released is to observe the force variation over a number of cycles. Table 1 presents this variation in the form of an index of variation (σ/μ- where σ and μ represent rms and mean value respectively) for the positive and negative pressure peaks computed over subsequent cycles of surface pressure, normalised by the corresponding mean force value μ_f, for the three testing velocities U=5, 7.5, 10 m/s.

The resulting index of variation I_v is close to zero for all wind speed which indicates there is little cycle to cycle variation in the peak pressures, and suggests there is no multi-cycle vortex shedding. Lugt (1983) suggested that a rapidly rotating plate would release a vortex after several revolutions (super-harmonic modes), whilst a slow rotating plate would not affect the shedding frequency (sub-harmonic mode) in which case the vortex shedding frequency would approach that value of a static plate. The intermediate lock-in case seems to be represented in this experiment. Fig. 9 shows very high normal force coefficients, which according to the values presented in Table 1 are likely to be caused by vortices released at every cycle, building in this way the moment coefficient scenario presented in Fig. 14.

5. Discussion of magnified coefficients

Tachikawa (1983) suggested a method for the computation of magnified pressure coefficients. These were expressed as the sum of the average and fluctuating part of an assumed Magnus effect. The average value depended on the frequency of rotation whilst the dynamic part was approximated by the difference between the corresponding static coefficient at a given position with

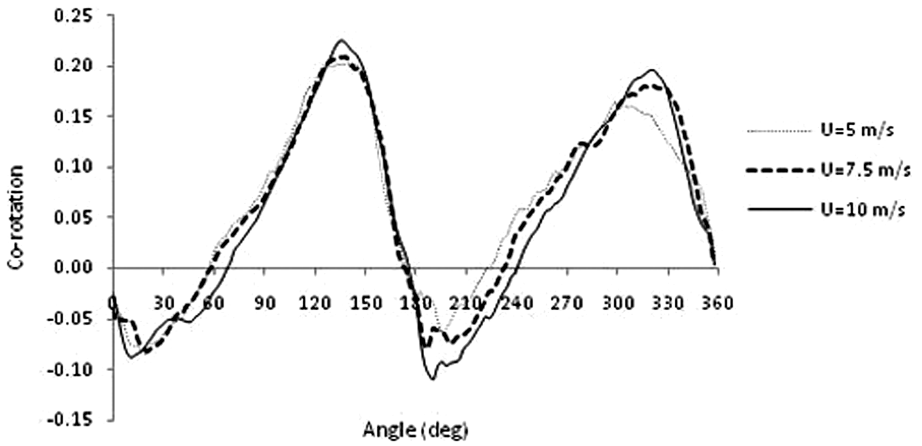

Fig. 15 Co-rotational mechanism, U = 5, 7.5, 10 m/s

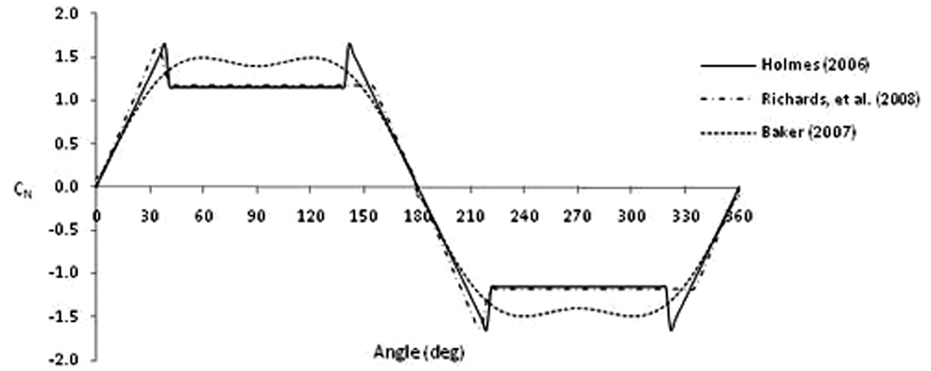

Fig. 16 Normal force coefficient after Holmes (2006), Baker (2007), and Richards, *et al*. (2008)

regard to the wind velocity and the average static value during a cycle. The case of interest here is that of stable auto-rotation, i.e., $C_{Qr}/C_{Qr0}=1$, $C_{Mr}=0$ given that $\omega/\omega_0=1$ in Tachikawa's (1983) Eq. (5). The expression for this particular case is given in Eq. (2) where c_{Kr0} is the K force coefficient determined under stable autorotation as indicated by the sub-index $r0$ and C_{Ks} is the corresponding static. Tachikawa suggested $C_{Dr0}=1.19$, and $C_{Lr0}=0.41$ for a square shape.

$$C_D = C_{Dr0} + C_{Ds} - \overline{C}_{Ds} \;;\; C_L = C_{Lr0} + C_{Ls} \;;\; C_M = C_{Ms} \tag{2}$$

Holmes, *et al*. (2006), Baker (2007), and Richards, *et al*. (2008), have all suggested values for normal pressure coefficients. Baker (2007) has also given explicit expressions for drag, lift and moment coefficient, whilst Richards, *et al*. (2008) ignored the stall region for angles adjacent to 150° and 330°. Figs. 16~19 below show how these three approaches compare.

Based on the force coefficients presented in Figs. 16~19, the magnified values determined with Eq. (2) have been calculated, and are presented in Figs. 20~23. These figures also include the corresponding coefficients that resulted from the present experiment. Holmes, *et al*. (2006), Baker (2007), and Richards, *et al*. (2008) are now referred in their magnified form as Holmes-Tachikawa,

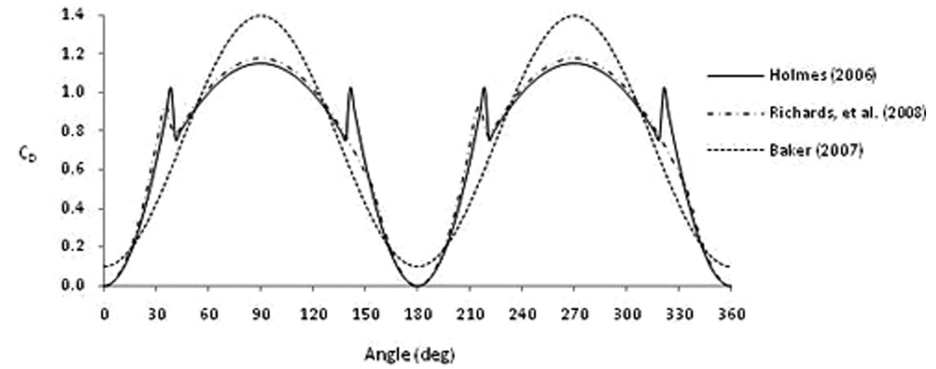

Fig. 17 Drag coefficient after Holmes (2006), Baker (2007), and Richards, *et al.* (2008)

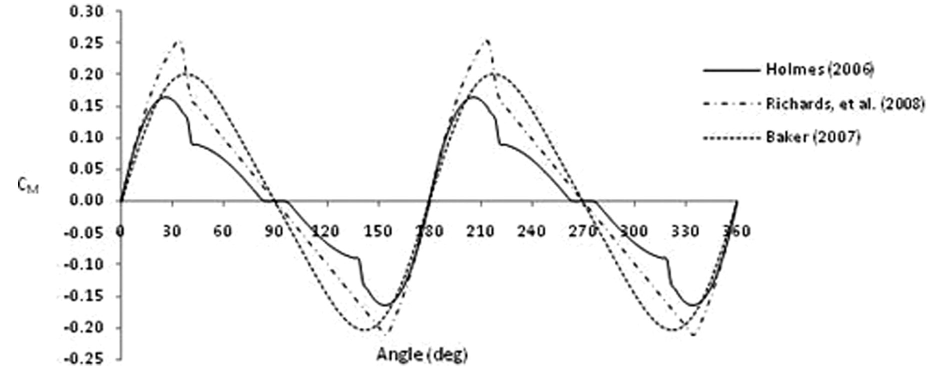

Fig. 18 Moment coefficient after Holmes (2006), Baker (2007), and Richards, *et al*. (2008)

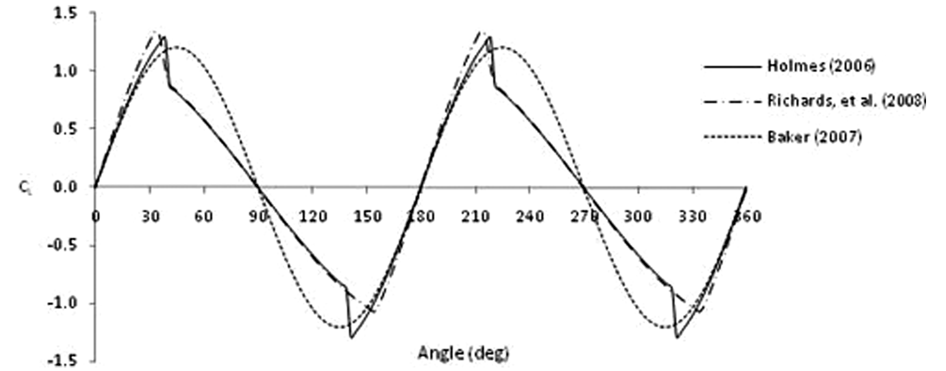

Fig. 19 Lift coefficient after Holmes (2006), Baker (2007), and Richards, *et al*. (2008)

Baker-Tachikawa, and Richards, *et al*.-Tachikawa, respectively. The superscript M in the new notation (i.e. C_M^M) refers to the magnified form.

A difference in drag coefficients observed between the experimental and classical approaches (Fig. 21), will result in underestimations of velocities when computing flight trajectories using the classic methods. The underestimation of drag forces in the intervals 60°~140° and 240°~320° is somewhat

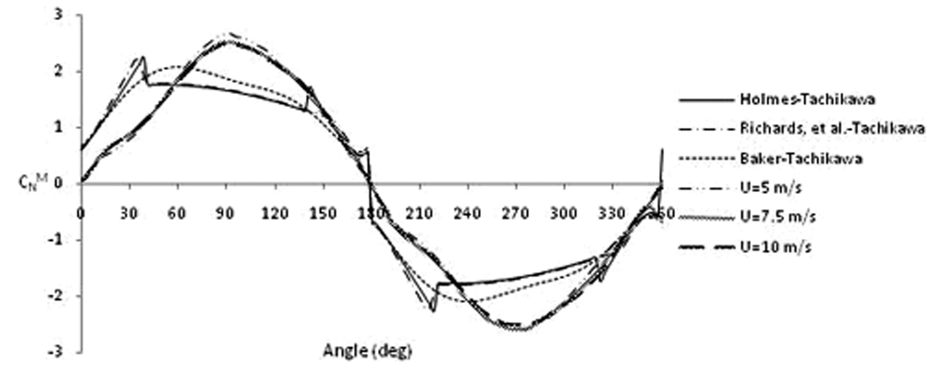

Fig. 20 Magnified normal coefficients compared to experimental results

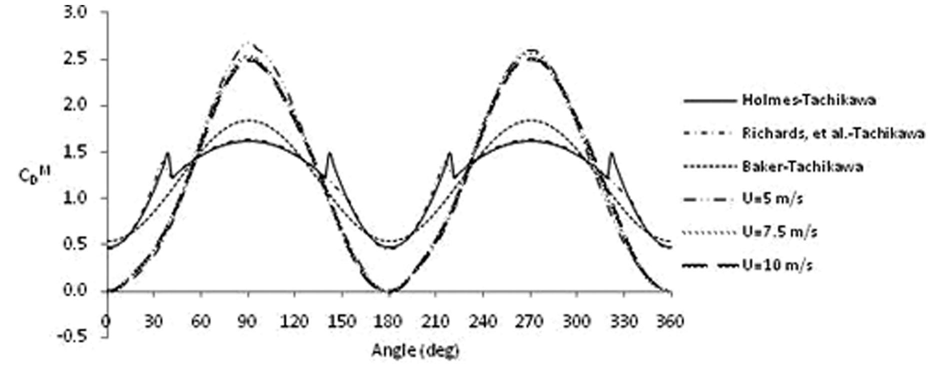

Fig. 21 Magnified drag coefficients compared to experimental results

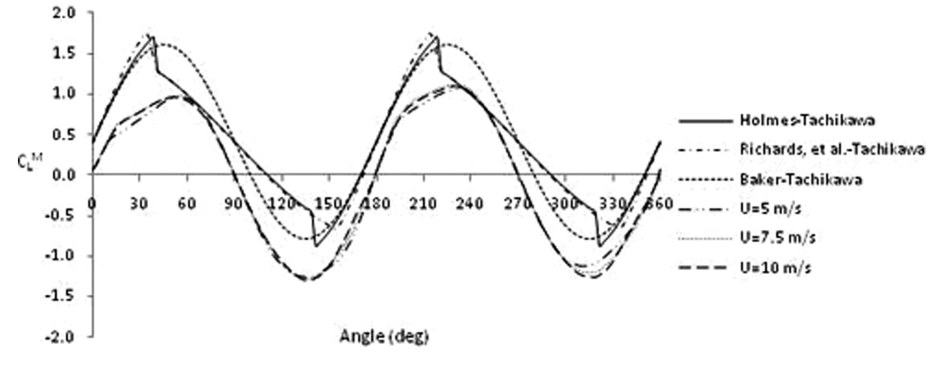

Fig. 22 Magnified lift coefficients compared to experimental results

compensated for by their overestimation at other angles of attack. Lift coefficients derived from the experiment do not reflect the asymmetries relative to zero values that result from the classic magnification method. The moment coefficients obtained through the present experiment (even though they are affected to some degree by frictional effects at the bearings) show significant differences in relation to values computed through existing approaches magnified using Tachikawa's method, all of which predict zero cumulative torque during a cycle.

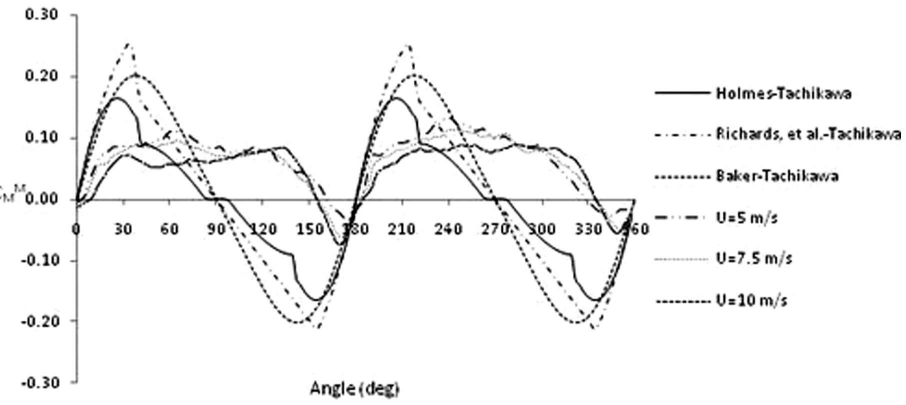

Fig. 23 Magnified moment coefficients compared to experimental results

6. Conclusions

Static and auto-rotating pressure coefficients derived from an experiment using a novel on-board system have been presented. In some respects the results seem to be consistent with data reported by other authors, while in other respects differences are considerable. In the case of static measurements the stall affect appears in the experimental data in similar intervals of pitch angles to previous experiments. In this case the peak normal coefficient oscillates between 1.2 ~ 1.3 in the stall region and between 1 ~ 1.1 for angles above 45° for the two testing velocities (U= 5, 10 m/s). A broad range of combinations of pitch and yaw angles seem to confirm the stall and steady region for static coefficients. With regard to autorotation, high values of normal pressure were recorded apparently due to a lock-in effect occurring between vortex shedding frequency and the frequency of rotation of the board. This hypothesis is supported by a low index of variation of areas under positive and negative peaks which indicates that all mechanisms that generate auto-rotational forces are present in every cycle at similar rates. Until now, auto-rotational moment coefficients have been inferred by using measured forces and assuming the position of the centre of pressures as determined from static measurements (quasi-steady approach). As illustrated, this results in a moment coefficient which does not match the present experimental measurements. It is suggested here on a heuristic base that quasi-steady torque is coupled with what has been termed a co-rotation and that these two mechanisms would define total torque. At this point however, there is no numerical or experimental argument to affirm that total forces derived from net pressures act on each of these mechanisms at the same level. The same would apply if we used forces determined through static tests acting on the quasi-steady mechanism only, since, as it has been shown during the present analysis, the forces derived from static and auto-rotational conditions does not seem to be determined by the same physical phenomena. In order to clarify this point it is necessary to undertake more detailed analysis, such as principal or independent component analysis, through which a more refined description of the force-mechanisms involved in autorotational events can be estimated. Finally, the magnification approach given in Tachikawa (1983) has been revisited in the second part of this paper. It was observed that experimental data compares fairly well to force coefficients computed as in Holmes, *et al.* (2006), Baker (2007), and Richards, *et al.* (2008), magnified using Tachikawa's method. There are some differences for drag coefficients which appear underestimated by classical approaches in the range of angles of attack between 60º ~ 120º and 240º ~ 300º, although these are overestimated elsewhere. Moreover, experimental data reports a lack of symmetry for the lift coefficient with regard to zero values; this differs from Tachikawa's approach which clearly predicts asymmetries in the lift forces due to the Magnus effect. With regard to magnified moment coefficients computed throughout the classic approach, these results in an accumulated momentum during a cycle equalling zero, i.e. no autorotation would be predicted through them.

Acknowledgements

Funding for this research was provided by the Engineering and Physical Sciences Research Council - grant number EP/F03489X/1. The authors wish to express their gratitude to Mr. M. Vanderstam of the University of Birmingham for help with the construction of the experimental set.

References

Baker, C.J. (2007), "The debris flight equations", *J. Wind Eng. Ind. Aerod.*, **95**, 329-353.

Cohen, M.J. (1976), "Aerodynamics of slender rolling wings at incidence in separated flow", *AIAA J.*, **14**, 886-93.

Daniels, P. (1970), "A study of the nonlinear rolling motion of a four-finned missile", *J Spacecraft Rockets,* **7**, 510-512.

Flachsbart, O. (1932), "Messungen an ebenen und gewolbten Platten", *Ergebnisse der AVA*, IV.

Gnip, I.J., Veyelis, S.A., Kersilus, V.I. and Vaitkus, S.I. (2007), "Deformability and strength of expanded polystyrene (EPS) under short-term loading", *Mech. Compos. Mater.*, **43**(1), 85-94.

Holmes, J.D. (2004), "Trajectories of spheres in strong winds with application to windborne debris", *J. Wind Eng. Ind. Aerod.*, **92**, 9-22.

Holmes, J.D., Letchford, C.W. and Lin, N. (2006), "Investigation of plate-type windborne debris - Part II. Computed Trajectories", *J. Wind Eng. Ind. Aerod.*, **94**, 21-39.

Iversen, J.D. (1979), "Autorotating flat-plate wings: the effect of the moment of inertia, geometry and Reynolds number", *J. Fluid Mech.*, **92**(2), 327-348.

Lin, N., Letchford, C.W. and Holmes, J.D. (2006), "Investigation of plate-type wind borne debris. Part I, Experiments in wind tunnel and full scale", *J. Wind Eng. Ind. Aerod.*, **94**, 51-76.

Lugt, H.J. (1983), "Autorotation", *Annu. Rev. Fluid Mech.*, **15**, 123-47.

Martinez-Vazquez, P., Baker, C.J., Sterling, M. and Quinn, A.D. (2009a), "The flight of wind borne debris: an experimental analytical and numerical investigation: Part I (Analytical Model)", *Proc. of the Fifth European and African Conf. on Wind Engineering (EACWE5)*, 437-440.

Martinez-Vazquez, P., Baker, C.J., Sterling, M., Quinn, A.D. and Richards, P.J. (2009b), "The flight of wind borne debris: an experimental analytical and numerical investigation. Part II (Experimental work)", *Paper accepted for The Seventh Asia-Pacific Conf. on Wind Engineering*, November 8-12, Taipei, Taiwan.

Neumark, S. (1963), "Rotating aerofoils and flaps", *J. R. Aeronaut. Soc.*, **67**, 47-63.

Riabouchinsky, D.P. (1935), "Thirty years of theoretical and experimental research in fluid mechanics", *J. R. Aeronaut. Soc.*, **39**, 282-348.

Richards, P.J., Williams, N., Laing, B., McCarty, M. and Pond, M. (2008), "Numerical Calculation of the 3-Dimensional Motion of Wind-borne Debris", *J. Wind Eng. Ind. Aerod.*, **96**, 2188-2202.

Tachikawa, M. (1983), "Trajectories of flat plates in uniform flow with application to wind-generated missiles", *J. Wind Eng. Ind. Aerod.*, **14**, 443-453.

Wills, J.A.B., Lee B.E. and Wyatt, T.A. (2002), "A model of wind-borne debris damage", *J. Wind Eng. Ind. Aerod.*, **90**, 555-565.

Appendix A – Method to transform time to angular coordinates

Considering inertial and frictional forces it can be shown that the following angular equation of motion is valid:

$$I\frac{d\omega}{dt} + k\omega = \frac{1}{2}\rho A h U^2 C_M(\theta) \tag{A.1}$$

where ω is the angular velocity, θ is the angular co-ordinate, t is time, I is the moment of inertia, k is a damping coefficient generated by frictional effects, ρ is the density of air, A is the plate area, h is the plate length, U is the free stream velocity and C_M is the pitching moment, which is a function of θ. Now defining:

$$\bar{\omega} = \omega T \ ; \ \bar{t} = \frac{t}{T} \tag{A.2}$$

where T is the period of rotation, one can write the equation as follows:

$$\frac{d\bar{\omega}}{d\bar{t}} + \frac{kT}{I}\bar{\omega} = \frac{\rho A h U^2 T^2}{2I} C_M(\theta) \tag{A.3}$$

Now Refining:

$$a = \frac{kT^2}{I} \ ; \ \beta = \frac{\rho A h U^2 T^2}{2I} \tag{A.4}$$

and letting the pitching moment form be given by

$$C_M(\theta) = \gamma(\sin(4\pi\bar{t}) + \delta) \tag{A.5}$$

(which is an approximation to experimental values), results in the equation:

$$\frac{d\bar{\omega}}{d\bar{t}} + a\bar{\omega} = \beta\gamma(\sin(4\pi\bar{t}) + \delta) \tag{A.6}$$

γ is the semi-amplitude of the pitching moment (approx 0.15), and δ is the offset of the mean from zero divided by the semi-amplitude (approx 0.15). Applying the following boundary

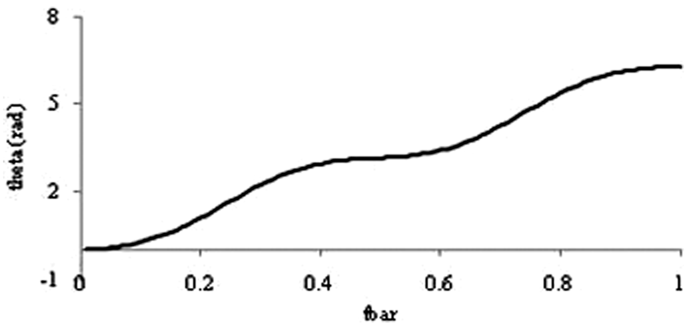

Fig. A1 Relationship between unitary time and angular position conditions (which simply state that the angular velocity is the same at the start and end of the cycle, and that the angular length of the cycle is 2π).

$$\omega_{\bar{t}=0} = \omega_{\bar{t}=1} \;;\; \theta_{\bar{t}=1} = \theta_{\bar{t}=0} + 2\pi \tag{A.7}$$

this equation has the solution:

$$\theta_{\bar{t}} - \theta_{\bar{t}=0} = 2\pi\bar{t} - \frac{\beta\gamma}{\alpha^2 + 16\pi^2}\left(\sin(4\pi\bar{t}) + \frac{\alpha}{4\pi}\cos(4\pi\bar{t}) - \frac{\alpha}{4\pi}\right) \tag{A.8}$$

Also the boundary conditions result in the identity:

$$\alpha = \frac{\beta\gamma\delta}{2\pi} \tag{A.9}$$

which implies the offset on the pitching moment coefficient curve (δ) represents the torque required to overcome frictional effects (α). Fig. A-1 shows the rotational speed computed through this method, for a cycle with unitary period.